LRP 624/98 December 1998

Papers presented at the

International Conference on
Fusion Reactor Materials - 8

Sendai, Japan
October 26 - 31, 1997

Accepted for publication in:
"Journal of Nuclear Materials"

LIST OF CONTENTS

Chemical segregation behavior of the low activation ferritic/martensitic steel F82H

R. Schäublin, P. Spätig and M. Victoria

EURATOM Association-Swiss Confederation, CRPP-EPFL, 5232 Villigen PSI, Switzerland

Abstract

The microstructure of the low activation F82H ferritic/martensitic steel has been investigated in the case of the heat treated and irradiated material. The irradiation has been achieved with 590 MeV protons in the PIREX facility to a dose of 0.5 dpa at a temperature of 523 K. The mechanical properties being intrinsically related to the chemistry of the metal, the understanding of the segregation behavior of the different alloying elements to microstructure defects, such as boundaries, is crucial. The segregation behavior to irradiation of both martensite laths and pre-austenite grain (PAG) boundaries is investigated using energy filtered transmission electron microscopy (EFTEM). It appears that Fe depletion of boundaries is observed in all cases, and the heat treated material experiences Cr segregation to boundaries, while the irradiated material experiences Cr depletion.

1. Introduction

Ferritic/martensitic steels have proved to be good alternatives to austenitic steels as candidates for the future fusion reactor structural components where doses above 100 dpa are expected. The chemical composition of the ferritic/martensitic steel F82H has been designed to obtain a reduced long term radioactivity. There is however a number of questions related to the changes in mechanical properties and to the swelling under irradiation that are still not fully answered. Recent studies on irradiation embrittlement of some ferritic steels have revealed that considerable shifts in the ductile-brittle transition temperature (DBTT) due to neutron irradiation appear together with an intergranular fracture mode [1]. This grain boundary embrittlement has been considered in [2] to be due to grain boundary precipitation of Mn and Si. Cr segregation to the pre-austenite grain (PAG) boundaries, and presumably to the martensitic lath boundaries as well, induced by the heat treatment prior to irradiation is believed to strengthen the boundaries [3]. It appears that irradiation depletes the grain boundaries of Cr, like in Fe-Ni-Cr stainless steels [3] and in commercial stainless steels [4], and it was shown in a ferritic steel Fe-Cr-P that Cr depletion of grain boundaries enhances the intergranular fracture mode [5].

A comparative study of the Fe and Cr segregation at grain boundaries is made here on the ferritic/martensitic F82H steel heat treated and specimens irradiated to 0.5 dpa with 590 MeV protons at a temperature of 523 K in the PIREX (Proton IRradiation EXperiment) facility located in the Paul Scherrer Institute of Villigen in Switzerland. The focus of this paper is on the chemistry of both martensite laths and grain boundaries. The mechanical properties and the microstructure investigation are presented elsewhere [6,7]. Although interface chemistry has been investigated with AES and using the sub-nanometric electron probe approach with EDS and (P)EELS in the past, the prospect of improving the spatial resolution, as well as preventing local changes in chemistry and low spatial statistics that are inherent to the probe approach, makes the use of EFTEM (Energy Filtered TEM) an attractive option. Moreover, the success of this technique in the study of Si segregation to grain boundaries in Cu [8] preceeds its use in the present work.

2. Experimental

The ferritic/martensitic F82H steel contains 7.65 % Cr, 2 % W, and Mo, Mn, V, Ta, Ti, Si and C below 1 % in sum total, and Fe for the balance [9]. The standard heat treatment (0.5 h at a temperature of 1313 K for the normalization, followed by 2 h at 1013 K for the tempering) has been applied in order to condition the material.

The TEM samples in the form of 100 μm thick 3 mm disks were prepared by electrochemical thinning with a solution of 10 vol. % perchloric acid and 90 vol. % methanol at a temperature of 0 °C and a voltage of 30 V. TEM observations were conducted on a Philips LaB_6 CM20 operated at 200 kV, and the EFTEM observations were achieved on a Philips FEG CM300 operated at 300 kV and equipped with a GIF (Gatan Imaging Filter). Both microscopes belong to the Centre Interdépartemental de Microscopie Electronique of the EPFL of Lausanne in Switzerland. Part of the EFTEM observations were achieved on a JEOL 4000 FX equipped with a GIF and operated at 400 kV that is located in the Department of Materials Science and Metallurgy of the University of Cambridge.

The EFTEM used here applies the technique of the three windows method with a post column filter. It sorts with a slit, or window, the transmitted electrons by their energy after passing through a magnet that is located below the main screen. The chemical map is obtained by subtracting from the image obtained using the electrons corresponding to a characteristic inner-shell loss edge for the element of interest an extrapolated background image derived from two images taken before the edge. This is done pixel by pixel in the digitized data, and in principle, the resultant loss image will show enhanced contrast in the regions rich in the selected element. There are however some inherent drawbacks to the method when a resolution of the order of the nanometer is expected.

The primary problem is the presence of conventional diffraction contrast due to the defect at which potential segregation is being examined. The diffraction contrast changes with the change in the energy loss at which the image is taken [10]. Consequently, there is an artificial contrast added on the chemical map that arises from the variation in the diffraction contrast from one image to the other. In order to circumvent that problem Hofer and Warbichler [11] proposed to acquire the images under a rocking beam illumination, which will average the diffraction contract to such an extent that the variation in diffraction contrast between images taken at the three different energy losses will be negligible. Unfortunately, this technique could not be applied to the present magnetic steel. This is presumably because a beam tilt caused by a magnetic sample will imply a change in the optical quality of the electron beam which degrades the resolution of the image.

In order to reduce the diffraction contrast problem, it is proposed here to select an objective aperture large enough to contain the transmitted beam and the main diffracted beam. This reduces the diffraction contrast and hence the aforementioned artefact on the chemical map. It should be noted that a compromise has to be found between a large enough objective aperture size that may reduce diffraction contrast and a smaller size that allows to reduce spherical

aberration [10]. It should be noted that the alignment of the images has to be done as precisely as possible in order to avoid subtraction of regions that do not correspond to each other.

The elements which are expected in our case to segregate to boundaries are Cr, Mn and Si [2,3]. Table 1 shows the energies of the main edges that are present in the EELS spectrum of the heat treated F82H material. The Mn, with a L edge at 640 eV, cannot be mapped using the three window method because one of the pre-edge images overlap the Cr L edge. The lower edge energies (C K edge, Si K edge and Mo M edge) prevent them to be used for mapping without difficulties because of the plasmon losses in this energy range that add to the signal and disturb the background extrapolation. The higher edge energies (Si L edge, Mo L edge and W M edge) present difficulties because the electron count rate is low and the acquisition times being higher the risk of sample drift and hence image blur is increased. The most suitable elements for chemical mapping are the Fe and the Cr. Their mapping was achieved using an energy window of 30 to 50 eV, with the L edge situated respectively at 708 eV and 574 eV, and with an acquisition time for the image of about 30 s. The three windows were taken at 495 eV, 545 eV for the two pre-edge images and 600 eV for the post-edge image for the Cr, and at 643 eV, 683 eV for the two pre-edge images and 733 eV for the post-edge image for the Fe.

3. Results and discussion

Figure 1, presented more in detail elsewhere [7], shows on low magnification micrographs the general microstructure of the F82H as heat treated (fig. 1(a)) and irradiated (fig. 1(b)). Both specimens have a common microstructure characterized by PAG boundaries and martensite lath boundaries.

In the following the chemical mapping results obtained by EFTEM of Fe and Cr at boundaries are presented. Fig. 2 presents the heat treated specimen and fig. 3 shows the 0.5 dpa irradiated specimen. In the unirradiated specimen segregation of Cr is visible at lath boundaries as shown in fig. 2(c) whilst there is a depletion of Fe (fig. 2(b)). The diffraction contrast visible on the zero loss image (fig. 2(a)) due to stress induced thin foil distortion is successfully reduced on both chemical maps. This can be seen for instance for the large black region below the interface on its left (fig. 2(a)) that cannot be distinguished anymore on the chemical maps (fig. 2(b) and (c)). The technique suggested here on the choice of the objective aperture proves to be successful, although there is still some residual diffraction contrast differences that add to the chemical signal as is observed when comparing the upper right corner of the zero loss image and the Cr map. It has to be noted that this residual contrast might be due to the drift of the sample during the acquisition of the images needed for the three window

method. This is illustrated in fig. 2(b) (Fe map) that presents a darker upper region relatively to the lower region, showing that the substraction of the extrapolated image and the post edge image was not achieved on regions corresponding exactly, contrary to the case of fig. 2(c) (Cr map) that presents no such drift trace. Moreover, the interface contrast of fig. 2(b), showing depletion by a dark contrast, is underlined by a slighty lighter contrast that is not related to the chemistry but to drift. This slight drift effect has no influence on the conclusion because the integral of the count rates in the darker region is higher than in the lighter region of the interface, stressing the fact that there is depletion.

As mentioned earlier, there is a compromise to be found in the choice of the objective aperture with regard to diffraction contrast and resolution. Another issue that is of practical importance is that the diffraction contrast is helpful to indicate the presence of thin interfaces. The fact that the interfaces present principally a diffraction contrast makes them difficult if not impossible to track them when the objective aperture is completely removed. But, again, even though diffraction contrast is helpful it has to be reduced to a minimum to avoid a perturbation of the chemical signal.

The irradiated specimen presented in fig. 3 exhibits on a boundary a dark line in the Fe map (fig. 3(b)). That indicates boundary Fe depletion. The Cr map (fig. 3(c)) of the same boundary shows a dark line. Although the image contrast of fig. 3(c) does not clearly display this dark line because of its noisiness, the image profile insert shows a significant intensity decrease at the boundary. This indicates boundary Cr depletion. The noisier image relatively to the heat treated case presented in fig. 2(c) taken with the same experimental acquisition conditions suggests that the amount of depletion is lower than the amount of segregation observed prior to irradiation. This Cr depletion may explain that intergranular fracture mode is observed after irradiation [1]. Fig. 3 shows in the upper right corner of the three images a large and dark feature. Its dark contrast in the Fe map (fig. 2(b)) and light contrast in the Cr map (fig. 3(c)) suggest that it is a Cr carbide.

An in-situ TEM tearing experiment has been conducted in order to observe the movement of a crack in relation with the microstructure features. By applying a rapid tilt to the sample holder the induced stress on the sample due to its immersion in the magnetic field of the objective lens allowed to bend the thin regions of the sample to such an extent that a crack could be initiated at the edge of the sample. The crack was then propagated progressively through the sample by further rapid tilts.

Figure 4 shows the in-situ TEM tearing experiment achieved on the as-received specimen. The crack visible in fig. 4(a) runs close to the martensite lath boundary labelled 2. Interestingly, it seems that the crack is not visibly influenced by the presence of the carbides

that are present on this martensite lath boundary. If the carbides are thought as being weakening points [12], the crack would then follow the martensite lath boundaries, leading to an intergranular fracture mechanism. It appears that this mechanism cannot be applied to explain the result of the present experiment. Effectively, even though the martensite lath boundary labelled 1 seems on fig. 4(a) to be in the propagation direction of the crack, Fig. 4(b) shows that the crack did not follow the martensite lath boundary but turned downwards. In addition, the crack does not seem to follow any of the visible lath boundaries. This TEM in situ experiment showing that the boundaries in the heat treated material are resistant to tearing might be explained by a boundary strengthening due to the observed Cr segregation. It shows for the least that they are not weakened by this segregation.

The fact that the irradiated material exhibits both Cr and Fe depletion shows that there is at least one element that was not determined in the present study that is segregated to the boundaries. Further work is being continued in this direction and on samples irradiated at higher doses.

4. Conclusion

1. Nanometric resolution in EFTEM is hindered in boundary chemistry investigation mainly by both diffraction contrast and image drift. It is suggested to choose an appropriate objective aperture that reduces diffraction contrast by including at least one of the major diffracted beams. EFTEM was applied successfully to the measurement of boundary segregation.

2. EFTEM measurements show that the Cr segregates to both martensite laths and PAG's boundaries in the heat treated ferritic/martensitic F82H steel, while Fe is depleted from them. After irradiation at 0.5 dpa at 523 K Cr is depleted from the boundaries as well as Fe.

Acknowledgements

Prof. C. Humphreys is acknowledged for providing access to the JEOL 4000FX of the Department of Materials Science and Metallurgy of the University of Cambridge. Dr. C. Boothroyd is acknowledged for helpful interactions on the EFTEM application to this study.

References

[1] R. L. Klueh, D. J. Alexander, Journal of Nuclear Materials, 187 (1992) 187.

[2] A. Kimura, L(a). Charlot, D.S. Gelles, R. H. Jones, Journal of Nuclear Materials, 212-215 (1994) 725.

[3] S. Watanabe, N. Sakaguchi, K. Kurome, M. Nakamura, H. Takahashi, Journal of Nuclear Materials, 240 (1997) 251.

[4] S. Kasahara, K. Nakata, H. Takahashi, Journal of Nuclear Materials, 239 (1996) 194.

[5] C. Liu, K. Abiko, M. Tanino, Materials Science and Engineering A176 (1994) 363.

[6] P. Spätig, R. Schäublin, S. Gyger, M. Victoria, this volume.

[7] R. Schäublin, P. Spätig, M. Victoria, this volume.

[8] R. E. Schäublin, W. M. Stobbs, Inst. Phys. Conf. Ser., 147, 3 (1995) 199.

[9] M. Tamura, H. Hayakawa, M. Tanimura, A. Hishinuma, T. Kondo, Journal of Nuclear Materials, 141-143 (1986) 1067.

[10] R. E. Schäublin, W. M. Stobbs, Inst. Phys. Conf. Ser., 147, 3 (1995) 203.

[11] F. Hofer, P. Warbichler, Ultramicroscopy, 63 (1996) 21.

[12] C. L. Briant, Materials Science and Technology, 5 (1989) 138.

Figure Caption

Figure 1 : TEM micrographs showing the basic microstructural features of the F82H material (a) heat treated, (b) irradiated at 0.5 dpa at 523 K.

Figure 2 : Chemical mapping of the heat treated F82H material. (a) Zero loss image, (b) Fe map and (c) Cr map. The inserts show the image profile integrated in the respective boxes outlined in white. Horizontal axis is in pixels, vertical axis in counts.

Figure 3 :Chemical mapping of the F82H material irradiated at 0.5 dpa at 523 K. (a) Zero loss image, (b) Fe map and (c) Cr map. The inserts show the image profile integrated in the respective boxes outlined in white. Horizontal axis is in pixels, vertical axis in counts.

Figure 4 : In situ TEM tearing experiment on the heat treated F82H material showing starting crack on (a) and on (b) cutted specimen. Arrows show two boundaries decorated with carbides.

Element	K	L	M	ΔE
Si	99.0	1839.0		*
Cr		574.0		30-50
Fe		708.0		30-50
Mn		640.0		*
Mo		2520.0	227.0	*
W			1809.0	*

Table 1 : Main EELS edges in [eV] in the ferritic/martensitic F82H steel. K, L and M energy lines are presented together with the energy window width (ΔE) used for the acquisition of the presented results. * : No corresponding chemical map acquired.

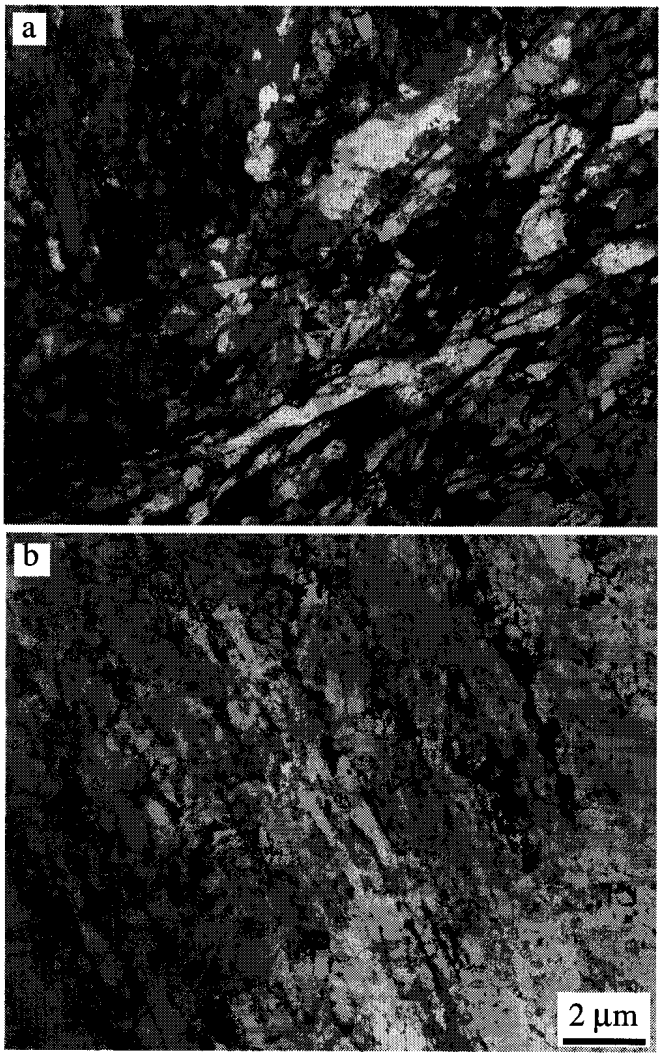

Fig. 1

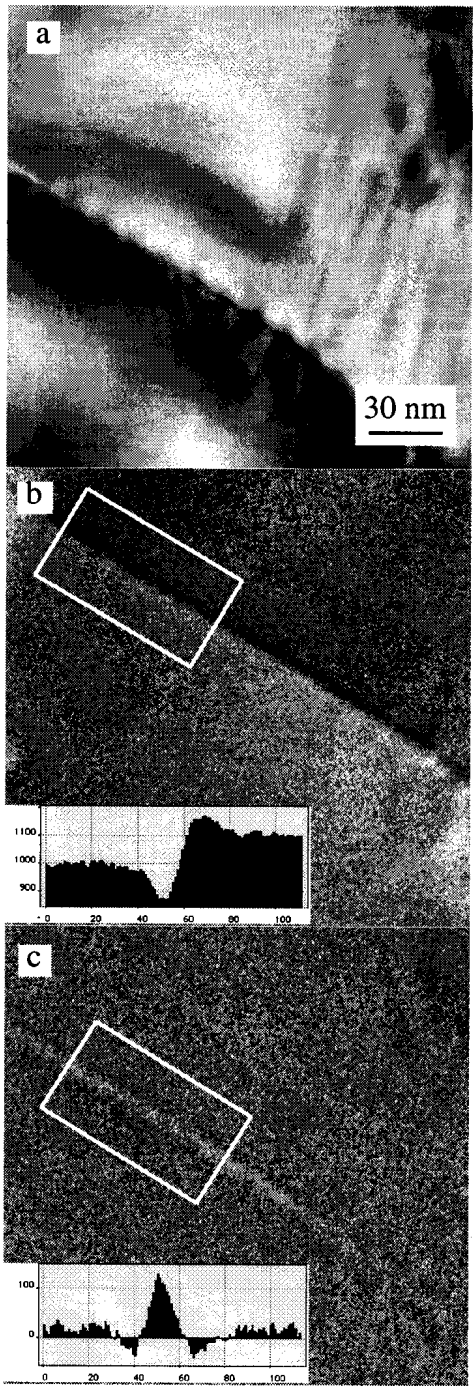

Fig. 2

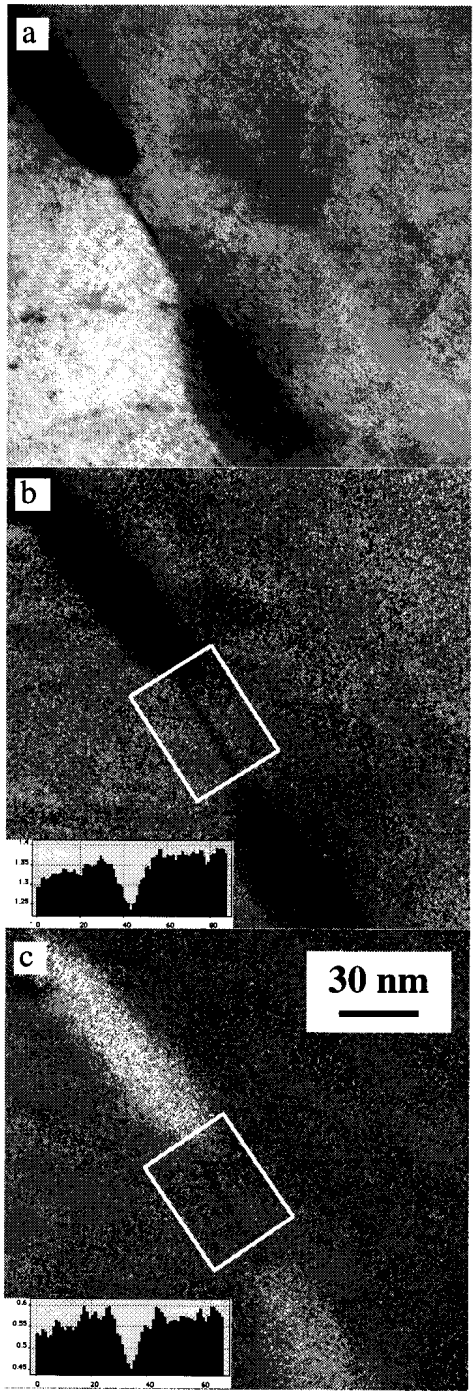

Fig. 3

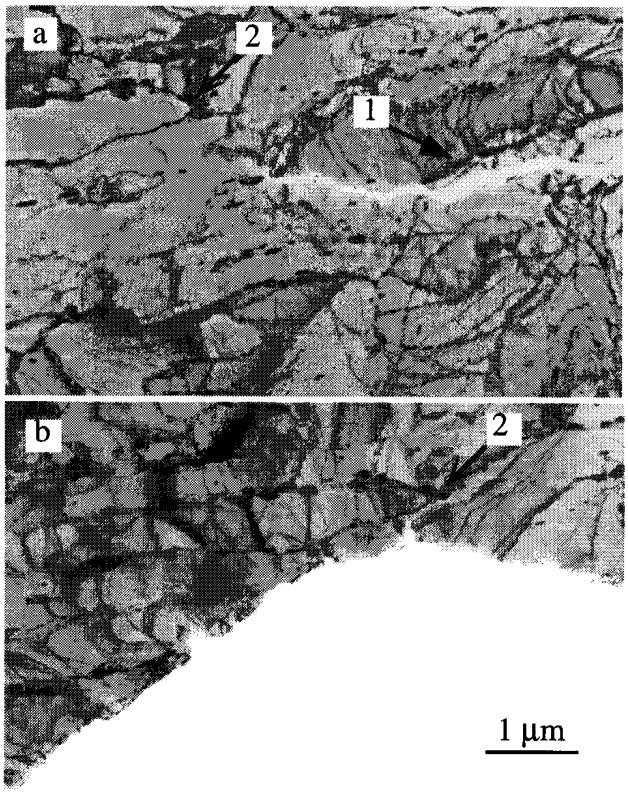

Fig. 4

Microstructure Assessment Of The Low Activation Ferritic/Martensitic Steel F82H

R. Schäublin, P. Spätig and M. Victoria

EURATOM Association-Swiss Confederation, CRPP-EPFL, 5232 Villigen PSI, Switzerland

Abstract

The microstructure of the low activation F82H ferritic/martensitic steel has been investigated in the cases of the heat treated, irradiated and deformed material. The irradiation has been achieved with 590 MeV protons in the PIREX facility to a dose of 0.5 dpa at a temperature of 523 K. The unirradiated material was deformed in tension to failure at room temperature. The dislocations character as well as the dislocations density are determined. The carbide chemical composition and the size distribution of the carbides are assessed.

Introduction

The ferritic/martensitic steels are candidates for the future fusion reactor structural components where doses above 100 dpa are expected. Even though these steels have proved to be a good alternative to austenitic steels, with respect to swelling resistance, there are a number of problems related to the changes in mechanical properties and to the activation under irradiation. In response to the latter point the chemical composition of the ferritic/martensitic steel F82H has been designed to obtain a reduced long term radioactivity. Owing to the complexity of the microstructure the mechanical properties are expected to depend on the chemical composition, the pre-austenite grain (PAG) sizes, the martensitic lath sizes, the carbide size distribution and composition, and the dislocation microstructure.

Irradiation is known to drive the microstructure to both the formation of He bubbles [1,2], and to a change in the dislocation configuration [2-5]. The He production rate for fusion 14 MeV neutron is 13 appm/dpa [6] and about 130 appm/dpa for 590 MeV protons, but the effect of the He on the mechanical properties is believed to be small [7,8]. H production is about 800 appm/dpa for 590 MeV protons [9] but rapidly escapes the material. The relative resistance of ferritic/martensitic steels to swelling which increases at a rate of about 1 % for 100 dpa [10] as compared to the 1 % for 10 dpa for austenitic steels has to be explained by the fact that the irradiation induced vacancies are impeded to form voids. Several models were proposed in that sense on the basis of (1) a trapping mechanism of the interstitial and vacancies to impurities and alloying elements [10] that increases recombination, (2) the trapping of both type of point defects on dislocations with a Burgers vector of a/2<111>, and (3) the point defect bias to dislocations being inherently lower in the bcc than in the fcc structure, the effect of the presence of dislocations with a Burgers vector equal to a<100> which trapping of interstitials leads to vacancy accumulation [4] is reduced. In the ferritic/martensitic steels the dislocation structure after irradiation develops dislocations with both a/2<111> and a<100> Burgers vectors, the latter being predominant when the Cr content is below the one of Fe-6Cr [2]. The a/2<111> is the most common Burgers vector in the bcc structure [10] whilst irradiation induced dislocations with the a<100> Burgers vector arises from the growth of a<100> interstitial loops [5].

A TEM study of the F82H microstructure is presented here. The mechanical properties and the chemical behavior of the F82H steel are presented elsewhere [11,12].

Experimental

The ferritic/martensitic steel denominated F82H [13] have a composition of about 7.65 wt. % Cr, 2 wt. % W, and Mo, Mn, V, Ta, Ti, Si and C below 1 wt. % in sum total, and Fe for the balance. The samples were submitted to the heat treatment (0.5 h at 1313 K for normalization and 2 h at 1013 K for tempering) that allows to obtain a fully martensitic structure.

The irradiation has been performed in the PIREX (Proton IRradiation EXperiment) facility located in the Paul Scherrer Institut of Villigen, Switzerland, with protons of 590 MeV at a temperature of 523 K to a dose of 0.5 dpa. The unirradiated sample was deformed in tension until failure on a Schenck RMC100 machine at 300 K. The TEM discs of the deformed specimen were taken from the uniform deformation region.

The 100 μm thick 3 mm TEM disks were prepared electrochemically (10 vol. % perchloric acid, methanol) at 0 °C and 30 V. Carbide size distribution measurement were achieved on extractions on carbon foils supported on Al grids. TEM observations and EDS measurements were conducted in the Centre Interdépartemental de Microscopie Electronique (CIME), EPFL, on a Philips LaB_6 CM20 operated at 200 kV. The high resolution observations were performed on a Philips FEG CM300 operated at 300 kV. The magnetism of the ferritic/martensitic steels requires particular attention to both objective astigmatism and beam tilt. The latter is corrected by recalling in diffraction mode the correct transmitted beam position recorded at the beginning of the session.

The carbide size distribution was investigated on both transmission and extracted samples. The dislocation Burgers vector were analyzed using the **g.b** analysis with a double-tilt side entry sample holder using the following procedure that provides four <011>-type **g**'s and two <200>-type **g**'s. The sample was tilted in order to reach a <111> zone axis, e.g. [111], that shows three different **g**'s of the <011> type, namely [10$\bar{1}$], [0$\bar{1}$ 1] and [1$\bar{1}$ 0]. From this zone axis one **g** is selected, e.g. [1$\bar{1}$ 0], and kept in order to reach by a 54.74° tilt of the specimen a <002> zone axis, e.g. [002]. The diffraction pattern is then composed of the [1$\bar{1}$ 0] **g**, its normal **g** = [110] and two <200>-type **g**, ([200] and [020]). The three known Burgers vector in bcc structure, i.e. 1/2 a_0 <111>, a_0 <100> and a_0 <110> [14], were accounted for in the analyses. The dislocation density was measured by counting the number of intersections of the dislocation with the free surfaces and by using the correction factors necessary to account for both the lack of visibility of a part of the dislocation population when using a given **g** diffraction vector and the unknown thickness [15].

Results and discussion

The micrographs of the general microstructure of the F82H heat treated (fig. 1(a)), deformed (fig. 1(b)) and irradiated (fig 1(c)) show common features characterized by both PAG

boundaries and martensite laths. The martensite laths are about 1 μm wide and can reach 10 μm in length as it is clearly visible on fig. 1(a). The lattice parameter of the heat treated F82H was measured with the diffraction patterns and the value averaged on three patterns obtained for different TEM sessions is 3.09 Å.

The dislocations in the heat treated F82H appear to be entangled (fig. 2), with the common to bcc structure burgers vector equal to 1/2 a_0 <111>. Neither a_0 <100> nor a_0 <110> Burgers vector were evidenced. The few straight segments appear to have a screw character. The deformed F82H contains dislocations that have a burgers vector equal to 1/2 a_0 <111> (fig. 3). Fig. 3(b) shows clearly that the dislocations are straighter than in the heat treated specimen. The character of the dislocation is screw. Dislocations in the irradiated F82H have a burgers vector equal to 1/2 a_0 <111> (fig. 4), with a dominating screw character.

The dislocation density in the heat treated, in the deformed and in the irradiated material is respectively 0.86×10^{10} dislocation/cm^2, 1.0×10^{10} dislocation/cm^2 and 0.9×10^{10} dislocation/cm^2, with a statistical error of ±20 %. Within the error margin there is no difference in the dislocation density between the three different specimens. These values are in agreement with those found in the literature [2, 3].

Carbides are present on the PAG boundaries, the lath boundaries and in the bulk of the martensite lathes. The carbides have an average composition of 60.6 at. % Cr, 28.8 at. % Fe, 6.3 at. % W, and traces in variable amounts of Ta, V and Ti. The carbides are close in composition to the common $M_{23}C_6$, that has an orthorhombic structure [16]. A CBED pattern analysis confirmed that the carbides have an orthorhombic structure. Furthermore it appears that bulk carbides are generally coherent with the matrix. Fig. 5 shows a HREM micrograph of the interface region between a bulk carbide of about 30 nm in diameter and the matrix. The power spectra shows that the <011> direction of the matrix is parallel to the <111> direction of the carbide. The white line shows that there is a common {011} plane between the matrix and the carbide. The {011} plane images shows that there is no mismatch dislocation in this direction between the two structures.

The carbide sizes range from 10 nm to 500 nm in all studied materials, for an average size of 43 nm, 47 nm and 49 nm for respectively the heat treated material (fig. 6(a)), the deformed (fig. 6(b)) and the irradiated material (fig. 6(c)). Hence the three studied material do not show significant changes within the statistical error in mean size or size ranges relatively to the heat treated material. The chemical composition of the carbides in the deformed and the irradiated material do no deviate from the ones in the heat treated sample. It should be noted that the peak in the small sizes of the carbide distribution is due to the relative large number of carbides with sizes below 10 nm. It does not reflect a bimodal size distribution.

The heat treated, deformed and the F82H material irradiated at 0.5 dpa at 523 K show similar dislocation configurations, with straighter screw dislocations for the deformed material. The carbide size distribution, mean size, composition and structure are equivalent within the three different materials. The similarity of the microstructure characteristics between the heat treated and the deformed specimens can be explained by the fact that the microstructure in the heat treated specimen contains a high residual internal stress induced by the heat treatment, even though the tempering temperature (1073 K) is chosen for a minimum of heat treatment induced hardening. It leads to a microstructure similar to the one derived from a deformation.

No irradiation defects such as dislocation loops or He bubbles were observed in the 0.5 dpa irradiated specimen, for the latter probably because of the relatively low irradiation temperature. Moreover, a close observation by weak beam TEM **g**(6**g**) with **g** = <011> showed that there is no irradiation induced precipitates, such as the chromium rich α' phase precipitates, as suggested in [2]. The lack of visible differences in the microstructure between the unirradiated and the irradiated specimen is certainly related to the relatively low dose explored so far in this study. However, chemical segregation behavior differences were observed between the unirradiated and the irradiated specimens [12].

Conclusion

The dislocation structure of the F82H ferritic/martensitic steel consists of 1/2 a_0 <111> Burgers vector dislocations. It appears that there is a strong tendency to screw character orientation in the unirradiated and specimens irradiated to 0.5 dpa, which suggests a Peierls mechanism.

No differences in either the carbide microstructure, composition or the size distribution were found between unirradiated and irradiated specimens.

Acknowledgments

Dr David Gelles is acknowledged for his advices on the observation in TEM of magnetic specimens.

References

[1] E. A. Little, D. A. Stow, Journal of Nuclear Materials, 87 (1979) 25.
[2] D. S. Gelles, Journal of Nuclear Materials, 108 & 109 (1982) 515.
[3] Y. Katoh, A. Kohyama, D. S. Gelles, Journal of Nuclear Materials, 225 (1995) 154.

[4] R. Bullough, M. H. Wood, E. A. Little, Effects of Radiation on Materials: 10th conference, ASTM STP 725, D. Kramer, H. R. Brager, J. S. Perrin Eds., ASTM (1981) 593.

[5] E. A. Little, R. Bullough, M. H. Wood, Proc. Roy. Soc. London, A372 (1980) 565.

[6] M. S. Wechsler, D. R. Davidson, L. R. Greenwood, W. F. Sommer, Effects of Radiation on Materials: 12th conference, ASTM STP 870, F. A. Garner, J. S. Perrin Eds., ASTM (1985) 1189.

[7] K. K. Bae, K. Ehrlich, A. Möslang, Journal of Nuclear Materials, 191-194 (1992) 905.

[8] K. Shiba, M. Suzuki, A. Hishinuma, J. E. Pawel, Effects of Radiation on Materials: Tenth conference, ASTM STP 1270, D. S. Gelles, R. K. Nanstad, A. S. Kumar, E. A. Little Eds., ASTM (1996) 753.

[9] S.L. Green, Journal of Nuclear Materials, 126 (1984) 30.

[10] E. A. Little, Journal of Nuclear Materials, 87 (1995) 11.

[11] P. Spätig, R. Schäublin, S. Gyger, M. Victoria, this volume.

[12] R. Schäublin, P. Spätig, M. Victoria, this volume.

[13] M. Tamura, H. Hayakawa, M. Tanimura, A. Hishinuma, T. Kondo, Journal of Nuclear Materials, 141-143 (1986) 1067.

[14] R. W. K. Honeycombe, The plastic deformation of metals, W. Clowes & Sons, London (1975) 111.

[15] P. B. Hirsch, A. Howie, R. B. Nicholson, D. W. Pashley, and M. J. Whelan, Electron Microscopy of Thin Crystals (Butterworths, London 1969), .

[16] J. H. Woodhead, A. G. Quarrell, Journal of The Iron and Steel Institute, 1965, 605.

R. L. Klueh, J.-J. Kai, D. J. Alexander, Journal of Nuclear Materials, 225 (1995) 175.

Figure caption

Figure 1 : TEM micrographs showing the basic microstructural features of the F82H material (a) heat treated, (b) deformed and (c) irradiated at 0.5 dpa at 523 K.

Figure 2 : **g.b** analysis of the heat treated F82H material. TEM micrographs taken with (a) g=[$\bar{1}$ 10], (b) g=[01$\bar{1}$] and (c) g=[10$\bar{1}$].

Figure 3 : **g.b** analysis of the deformed F82H material. TEM micrographs taken with (a) g=[$\bar{1}\bar{1}$ 0], (b) g=[200] and (c) g=[10$\bar{1}$].

Figure 4 : **g.b** analysis of the F82H material irradiated at 0.5 dpa at 523 K. TEM micrographs taken with (a) g=[$\bar{1}$ 01], (b) g=[$\bar{1}$ 10] and (c) g=[01$\bar{1}$].

Figure 5 : Coherency between the carbides and the matrix in F82H heat treated shown in a high resolution TEM micrograph (top image). Power spectra of the carbide (middle left) and of the matrix (middle right). The white line on the Fourier filtered enlarged image (bottom) indicates a common crystallographic plane.

Figure 6 : Carbide size distribution of F82H for the (a) heat treated material, (b) deformed material and (c) the material irradiated at 0.5 dpa at 523 K.

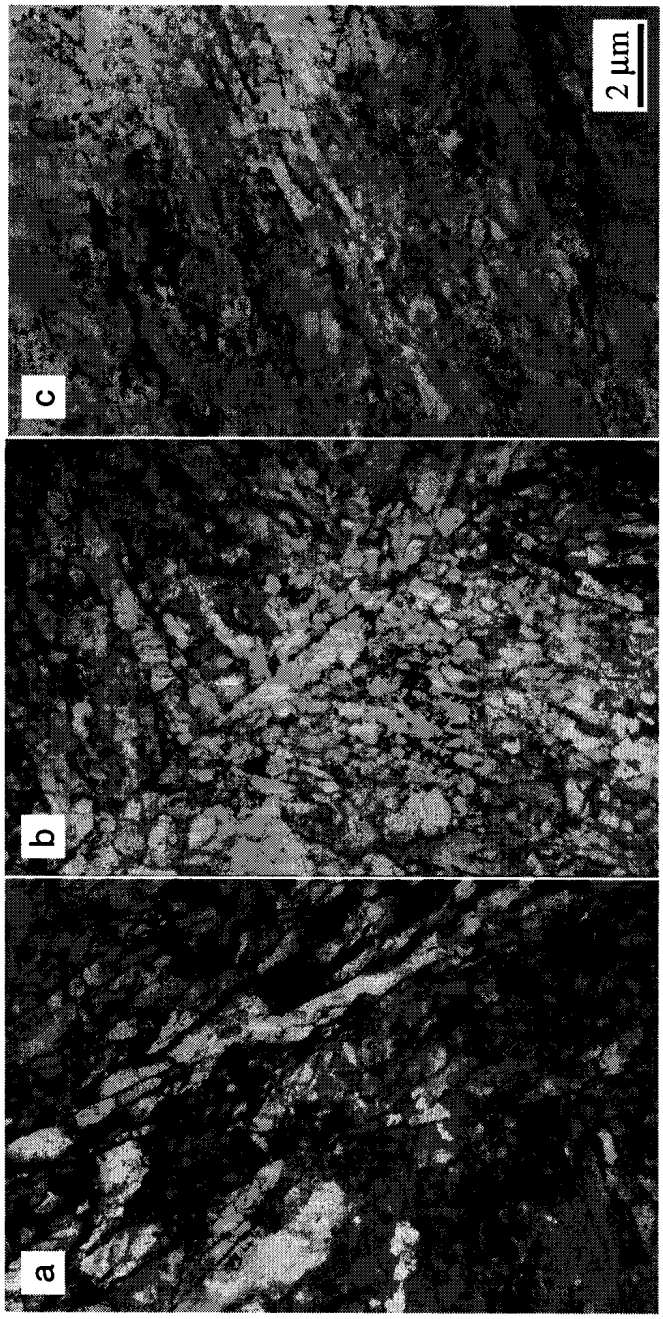

Fig. 1

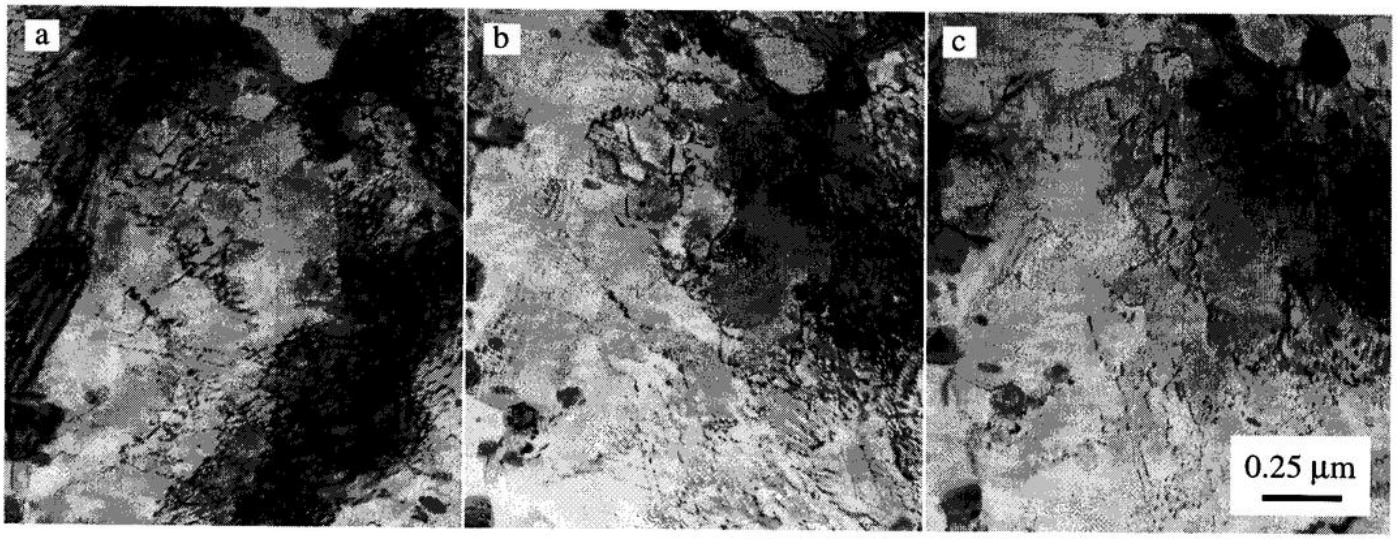

Fig. 2

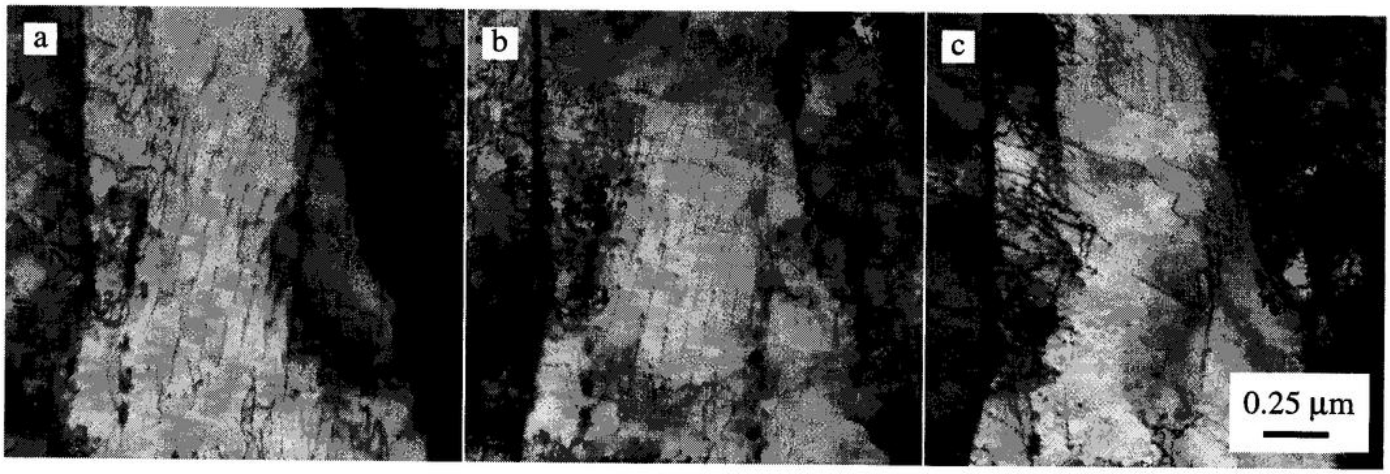

Fig. 3

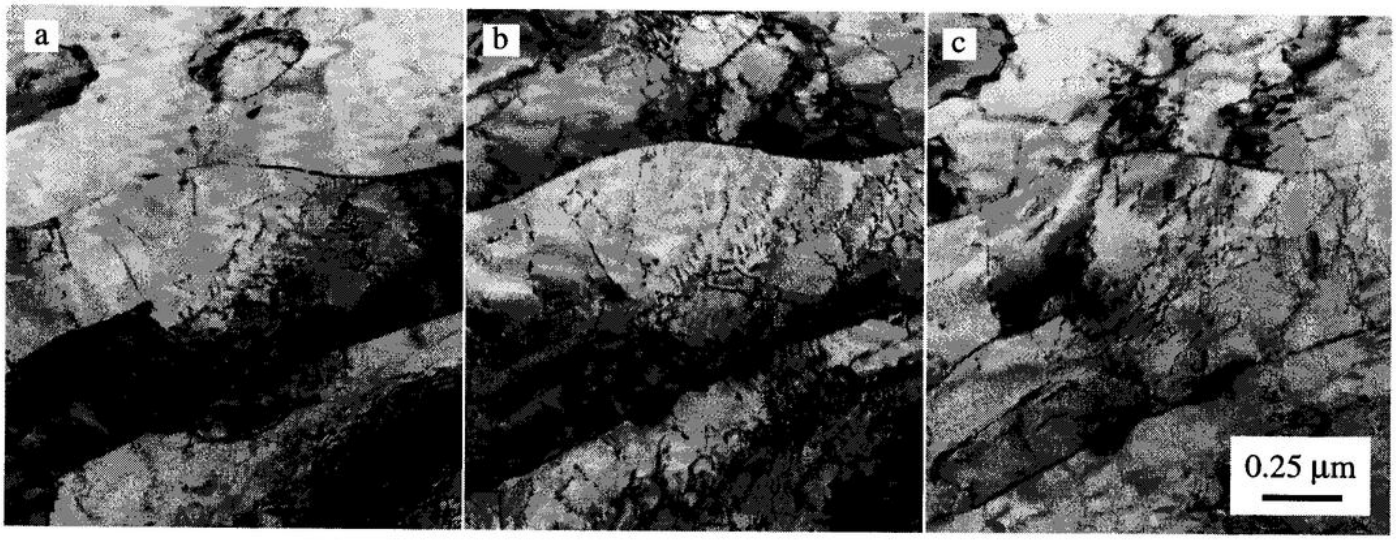

Fig. 4

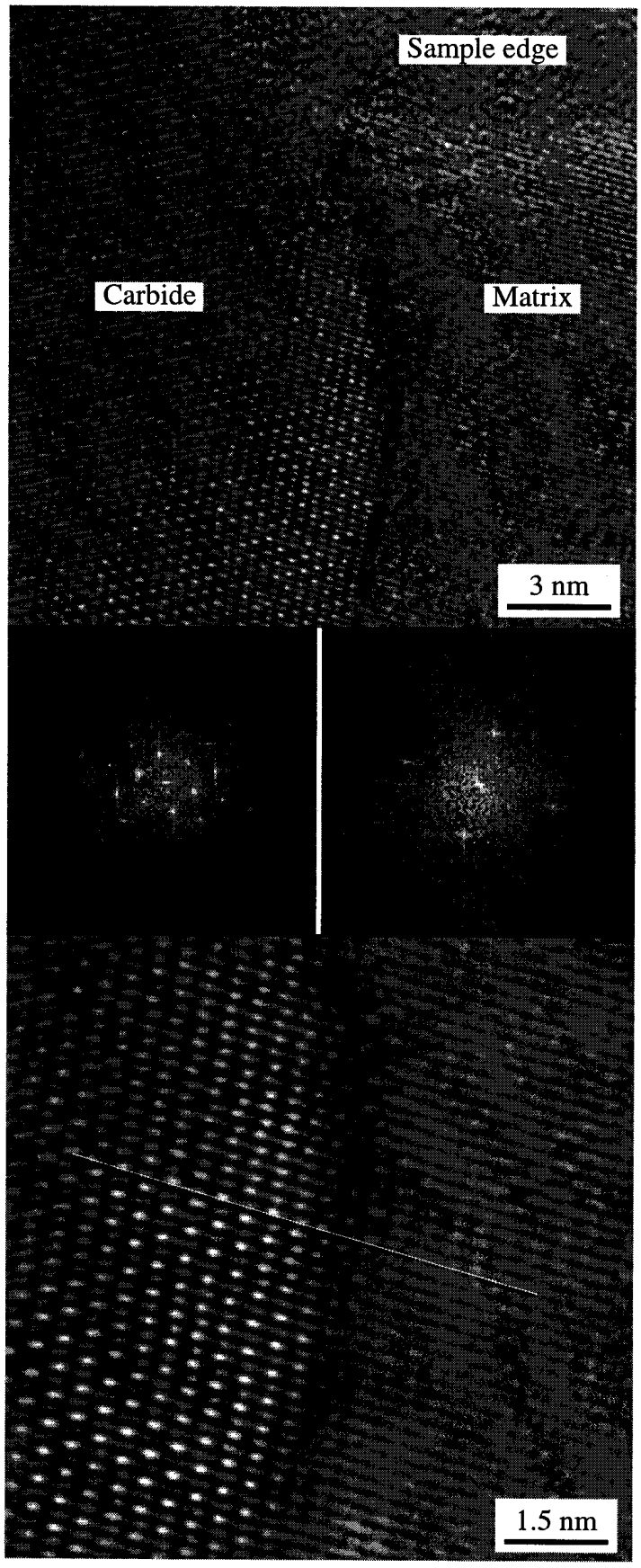

Fig. 5

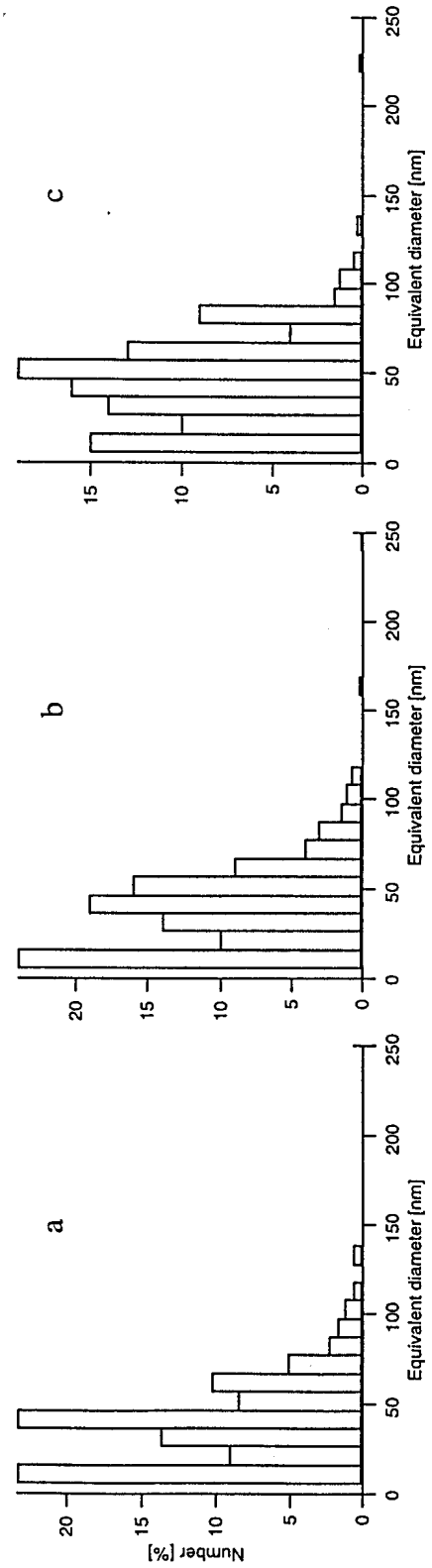
a
b
c
Number [%]
Equivalent diameter [nm]
Equivalent diameter [nm]
Equivalent diameter [nm]

Fig. 6

The mechanical properties of 590 MeV proton irradiated iron

Y. Chen, P. Spätig and M. Victoria

EPFL-CRPP Fusion Technology Materials, 5232 Villigen PSI, Switzerland

Abstract

The mechanical properties of 590 MeV proton irradiated pure α-iron have been investigated after irradiation at 320, 420 and 520 K to doses between 10^{-5} and 10^{-1} dpa. For comparison, corresponding tests were carried out on unirradiated iron specimens. Radiation hardening is observed at doses above 10^{-3} dpa for all irradiation temperatures and a $(\text{dose})^{1/4}$ dependence is found after irradiations at 320 K. It is shown that the irradiation suppresses the dynamic strain ageing observed in the unirradiated iron. The systematic observation of intergranular cracking in the specimens irradiated to doses of 10^{-3} dpa or larger is discussed in terms of dislocation channeling.

Keywords: iron, proton irradiation, radiation hardening, defects

1. Introduction

Much of the early work since the initial observations of radiation hardening [1] and defect microstructures resulting from neutron irradiation [2] in α-iron has been reviewed by Little [3], who pointed out the following mean features of the hardening: a $(\phi t)^{1/2}$ dose dependence, a damage saturation dose of ~ 10^{21}n cm^{-2} (E > 0.1 MeV) in pure iron and a strong effect of interstitial impurities. The defect structure after irradiation at reactor ambient temperature consists of small clusters or loops, probably interstitial in character. These observations have been confirmed more recently [4], after irradiation at higher temperatures (563 K) in both reactor and the RTNS II 14 MeV neutron source. Radiation softening has also been observed after irradiations at liquid helium temperatures and the annealing of this damage provides further indications of the interstitial nature of the irradiated damage microstructure [5-7].

The present investigation is part of a research program aiming at studying the possible effects of high energy recoils on the dose dependence and of microstructure and mechanical properties of pure metals and model alloys. These investigations are important for fusion materials because the recoil spectra of fusion neutrons has a mean energy much higher than that of fission reactor neutrons, which are the main irradiation media used at present, no intense 14 MeV neutron source being available. The PIREX [8] irradiation facility, with a beam of 590 MeV protons, is used for this purpose. The recoil spectra for protons of this energy has a maximum around 2-3 MeV in Fe [9]. It has already been shown that

in fcc pure metals irradiated at 320 K, no difference is found in the microstructures and tensile properties between the materials irradiated in PIREX and those obtained after fission or fusion neutron irradiations [10].

2.Materials and techniques

Foils, 250 μm thick, of 99.99 % pure iron were obtained from Goodfellow Cambridge Ltd. The main impurities, according to the nominal analysis provided by the supplier are B, Cr, Co, Cu, Ge, Mn, Ni and Si to a total of 100 wt.ppm and in addition 6.5 wt. ppm P and 3.8 wt. ppm S. No analysis of N was provided. The foils were annealed for 60 min. at 923 K under vacuum to obtain a grain size of 30 μm. Flat microtensile specimens, with a 8 mm gage length 2.5 mm wide, were spark-cut from the annealed foil. The specimens were finally lightly electropolished before testing or irradiation. Tensile testing was performed in a screw drive Schenck testing machine, at a constant crosshead velocity of 20 μm min^{-1}. Tests at room temperature were performed in air or in vacuum, while all tests at higher temperatures, up to 623 K, were performed in vacuum only. Stress relaxations were systematically performed during tensile testing in order to obtain values of the activation volume of the deformation mechanism.
Irradiations were performed in the PIREX [8] facility installed in a beam line of the 590 MeV proton accelerator at the Paul Scherrer Institute in Switzerland, at an average damage rate of $1.3x10^{-6}$ dpa sec^{-1}. The irradiation matrix included doses from 10^{-5} to 10^{-1} dpa at temperatures between 320 and 520 K.

3. Experimental results

3.1 Tensile tests

The microtensile specimens used in the present measurements have been shown to represent well the bulk tensile properties when the grain size is of the order of 30-50 μm. Only the total uniform elongation is smaller than that found in DIN type specimens [11].
Results from tensile testing at different temperatures of the unirradiated iron are shown in Fig. 1a. The lower yield strength at 423 K is comparable to that measured at 295 K, but the work hardening is much higher. At higher deformation temperatures both the yield strength and the work hardening decrease systematically, but the work hardening becomes lower than that obtained after room temperature testing only in the test at 623 K. Serrations in the flow stress are observed at all testing temperatures above room temperature and they are specially marked in the test at 423 K. The lower yield stress, measured in every case after the initial yield point, is plotted as a function of the test temperature in Fig 1b.
The tensile behaviour at room temperature with dose after irradiations at 320 K is shown in Fig 2a. No hardening is observed after 10^{-5} dpa and the corresponding work hardening is actually lower than that of the unirradiated specimen. The strain associated with the yield region (Luders band propagation) increases with dose and probably accounts for the total deformation at $8x10^{-2}$dpa, where practically no work hardening is observed. This is more clearly seen in the dose dependence at

423 K, shown in Fig 2b. The work hardening is almost linear and lower as the dose increases. Simultaneously, the serrations in the tensile curve disappear.
The dose dependence of the irradiation hardening $\Delta\sigma=\sigma_{irr}-\sigma_{unirr}$ is plotted in Fig 3. The data is not sufficient for a precise determination, but the present data fits well a $(dose)^{1/4}$ dependence after irradiations at 320 K. In the same figure, the effect of irradiation temperature on the dose dependence is also shown. The value $\Delta\sigma_T=\sigma^{irr}_{Ttest=Tirr}-\sigma^{unirr}_{Tirr}$ is plotted in this case, using the values corresponding to the lower yield strength. Again, the data set can only provide a trend showing the same $(dose)^{1/4}$ dependence as for the lower irradiation temperature.
As for the dependence of the room temperature lower yield stress with irradiation temperature, values for two doses are plotted in Fig. 4. The yield stress decreases with irradiation temperature, at a comparable rate for both dose levels.

3.2 The activation volume

Apparent activation volumes V_a were obtained from stress relaxations along the tensile curve, according to the relation [12, 13]:

$$\Delta\sigma_r = \frac{kT}{V_a}\ln\left(\frac{t}{C}+1\right)$$

where

$$C = \frac{MkT}{\dot{\varepsilon}_r V_a}$$

M is a constant determined from the stiffness of the testing machine and t is the relaxation time.
Because of the difficulty in establishing the correct stress level in strongly serrated tensile curves, the values of the activation volume show a larger dispersion than is normally observed, but trends can be clearly detected. As the serrations tend to disappear at higher stresses, a corresponding improvement in the scatter of the activation volumes is seen.
The activation volume values for three different doses at 320 K and those of the unirradiated specimen are shown in Fig. 5a, as a function of stress. Although the range of stress covered is not large enough, it can be seen that, except for the values obtained after 10^{-5} dpa, where no radiation hardening was found, the value of the activation volume of the irradiated specimens increase with stress towards the unirradiated asymptotic value of 125 b^3, where b is the Burgers vector. For higher temperature irradiations, the behaviour of the activation volume as a function of stress for both the irradiated and unirradiated material coincide, see Fig 5b. The asymptotic value of V_a at high stresses is ~ 40 b^3.

3.3 Surface observations

Scanning microscope observations were performed on the deformed specimens. Typical observations after room temperature deformation are shown in Fig. 6. While the unirradiated specimen, Fig 6a, shows only a microcrack starting to develop in the neck region, the irradiated specimen (T_{irr}= 320 K, 10^{-3} dpa) shows a distribution of microcracks over the gage length, Fig 6b. As can be seen in Fig 6c and 6d, these are produced mainly at grain boundaries and at triple points. In surface observations at different strains in an interrupted tensile test, the

microcracks are observed already after 12 % elongation at this particular dose and temperature.

4. Discussion

The presence of a large yield point and serrated yielding in the tensile curve at 423K is an indication that a mechanism of dynamic strain ageing (DSA) is operative, which is usually associated with the presence of interstitial impurities. Although C is below the ppm level, N was not analysed. It is also possible that the specimens could have picked up N during the vacuum anneal. It was very early recognised [14] that these extrinsic interstitials can combine with the irradiation produced defects, forming stable complexes, the creation of which reduces then the net concentration of interstitials in the lattice. Such mechanism implies that as the irradiation dose is increased, the DSA will disappear. This is readily observed in the specimens irradiated at 423 K after 10^{-2} dpa.

The observed irradiation hardening has been correlated in previous investigations with the presence of small clusters and loops of interstitial character, i.e. see [4]. No electron microscopy observations have been performed as yet in the proton irradiated iron, so there is no information on the characteristics of the proton irradiated microstructure. From the present results it can be inferred only a very small density of such defects is produced after proton irradiation to 10^{-5} dpa at 320 K, since no hardening has been observed under these conditions.

A comparison of the results of the present investigation can be made to those of the neutron irradiated iron samples produced out of the same batch as the ones used here. The dose dependence results from this investigation [15] have been included in Fig 3 and although the scatter is large, the trends are comparable after T_{irr}=320K. At higher irradiation temperatures, there are only two values for protons and two for neutron irradiation but neutrons seem to be more effective than protons in terms of hardening.

The trend of the activation volume of the irradiated material is consistent with the destruction of irradiation induced obstacles by the moving dislocation. After some amount of deformation the obstacle density decreases to the point were other obstacles (i.e. those pre-existing from the unirradiated state) control the deformation. It is unclear at this point what is the mechanism operative in the very low dose case (10^{-5} dpa), were the irradiation dose is not sufficient to produce a hardening defect microstructure

Although the activation volume data set at lower irradiation temperatures is still incomplete, it is clear from the strain/stress dependence of V_a after T_{irr}= 523 K that probably the operative rate controlling deformation mechanism is the same for the unirradiated and irradiated specimen.

Finally, the observed cracking localised at grain boundaries is believed to be associated with dislocation channeling: the dislocations sweep the irradiation produced defects as they move, so that it is easier for successive dislocation to glide in the same slip plane. This process leads to localised deformation by the formation of slip bands, in which several percent shear is accumulated. The localisation of such shear band at the grain boundary leads to the formation of the microcrack. The formation of dislocation channels has been observed after neutron irradiation [15].

6. Conclusions

(i) Radiation hardening is observed as a result of irradiation with 590 MeV protons at doses of 10^{-3} dpa or greater, in the 320 - 523 K temperature range.

(ii) The presence of DSA which is suppressed by irradiation to 6.4×10^{-3} dpa, is probably due to the presence of N.

(iii) A $(\text{dose})^{1/4}$ dependence is found at T_{irr}= 320 K, which is comparable to that obtained after neutron irradiation of iron of the same batch. At higher irradiation temperatures, hardening by neutron irradiation seems to be more effective.

(iv) Intergranular cracking has been systematically found in the irradiated iron at doses of 10^{-3} or higher. It is believed that this is an intrinsic mechanism of irradiated materials that deform by the dislocation channeling mode. Careful evaluation is needed of its effects on the small size specimens that are planned to be used in future fusion neutron sources.

Acknowledgements

The present research has been funded by the Swiss National Research Fund and the EU Fusion Technology Program.

References

[1] G.P. Seidel; Phys. Stat. Sol. 25 (1968) 175.
[2] B.L. Eyre; Phil. Mag. 7 (1962) 2107.
[3] E.A. Little; Int. Metals Rev. 21 (1976) 25.
[4] A. Okada, T. Yasujima, T. Yoshiie, I. Ishida and M. Kiritani; J. Nucl. Mater. 179-181 (1991).
[5] P. Groth, F. Vanoni and P. Moser; Proc. Int. Conf. On Defects and Defect clusters in bcc Metals and Alloys, Ed. R.J. Arsenault, AIME (1963) 19.
[6] K. Kitajima, H. Abe, Y. Ono, E. Kuramoto and S. Takamura, J. Nucl. Mater. 108 (1982) 436.
[7] H. Matsui, H. Shimidzu, S. Takehana and M.W. Guinan, J. Nucl. Mater. 155-157 (1988) 1169.
[8] P. Marmy, M. Daum, D. Gavillet, S. Green, W.V. Green, F. Hegedus, S. Proennecke, U. Rohrer, U. Stiefel and M. Victoria; NIM B 47 (1990) 37.
[9] M. Victoria, M. Alurralde, A. Caro, A. Horsewell and S. Proennecke; Materials Science Forum 97-98 (1992) 541.
[10] Y. Dai and M. Victoria; Proc. of the Symposium on Microstructure Evolution During Irradiation, I.A. Robinson, G.S. Was, L.W. Hobbs and T. Diaz de la Rubia Eds., MRS Vol. 439, p.319. See also Y. Dai, Thesis N^0 1388, Ecole Polytechnique Federale de Lausanne (1995).
[11] P. Spätig, R. Schäublin, S. Gyger and M. Victoria; Proc. this Conf. (ICFRM8).
[12] F. Guiu and P.L. Pratt; Phys. Stat. Sol. 6 (1964) 111.
[13] L.P. Kubin; Phil. Mag. 30 (1974) 705.
[14] G.P. Seidel, Rad. Effects 1 (1969) 177.

[15] B.N. Singh et al.; Proc. this Conf. (ICFRM8).

Figure Captions

Figure 1: (a) tensile behaviour of α-iron at different temperatures.
(b) Variation of the lower yield strength with temperature.

Figure 2: Tensile behaviour of iron irradiated to different doses
(a) tested at room temperature
(b) tested at the irradiation temperature

Figure 3: Irradiation dose dependence of the yield strength of iron. The neutron irradiation on the same batch of Fe is from [15].

Figure 4: Dependence of the yield strength with temperature at two different doses

Figure 5: Stress dependence of the apparent activation volume
(a) the effect of irradiation dose at room temperature
(b) the effect of irradiation at T_{irr}= 523 K

Figure 6: (a) cracking at the neck in the unirradiated specimen
(b), (c) and (d) intergranular cracking in the irradiated specimen, at different magnifications. 10^{-3} dpa at T_{irr} = 320 K

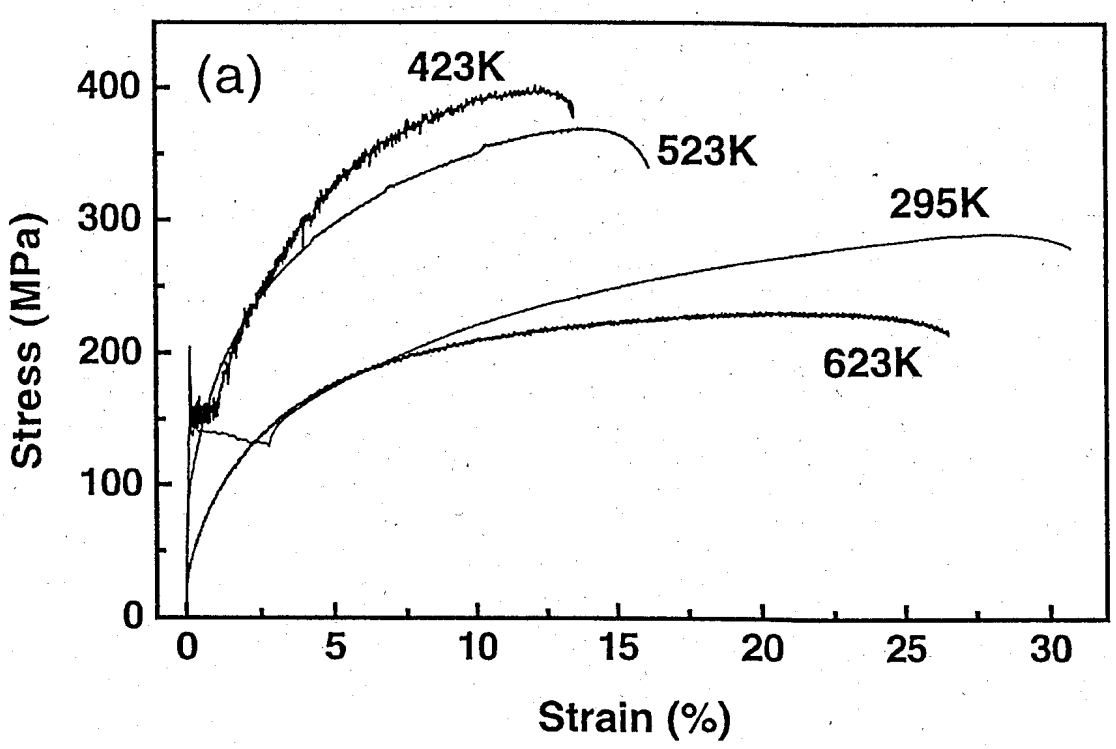
(a)
423K
523K
295K
623K
Stress (MPa)
Strain (%)
0
100
200
300
400
0
5
10
15
20
25
30

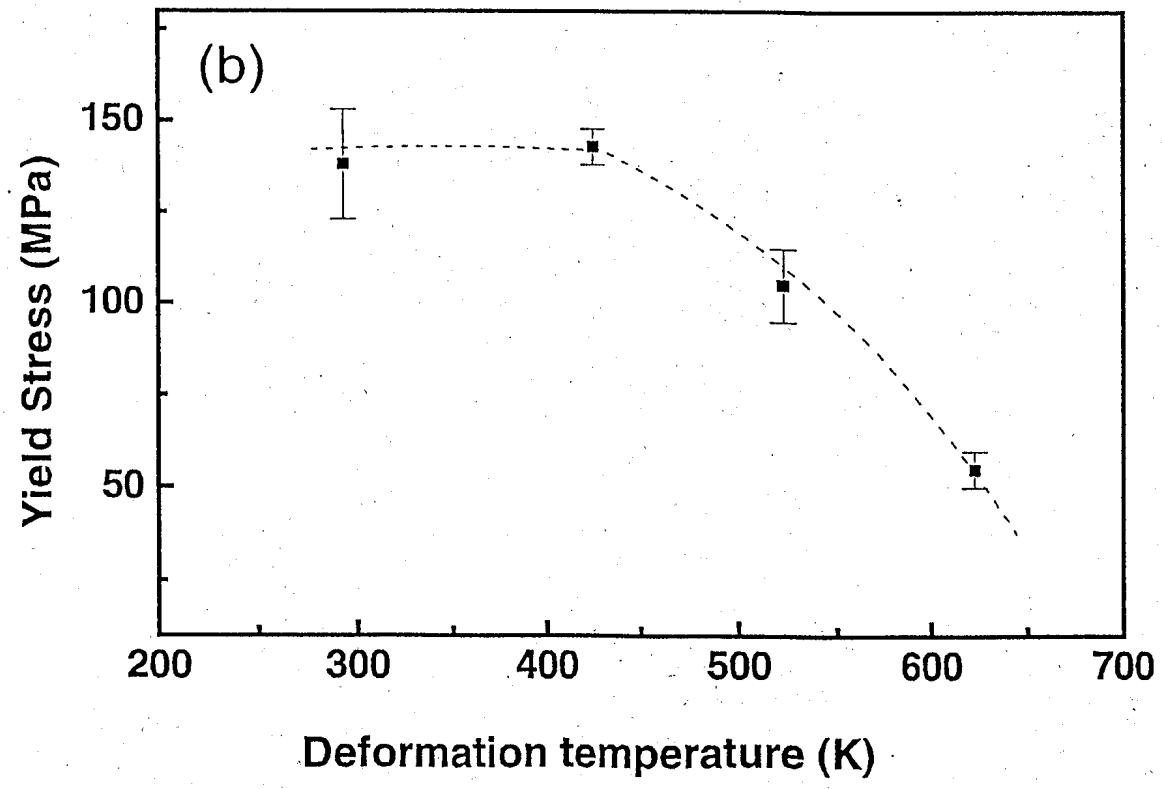
(b)
Yield Stress (MPa)
Deformation temperature (K)
50
100
150
200
300
400
500
600
700

Fig. 1

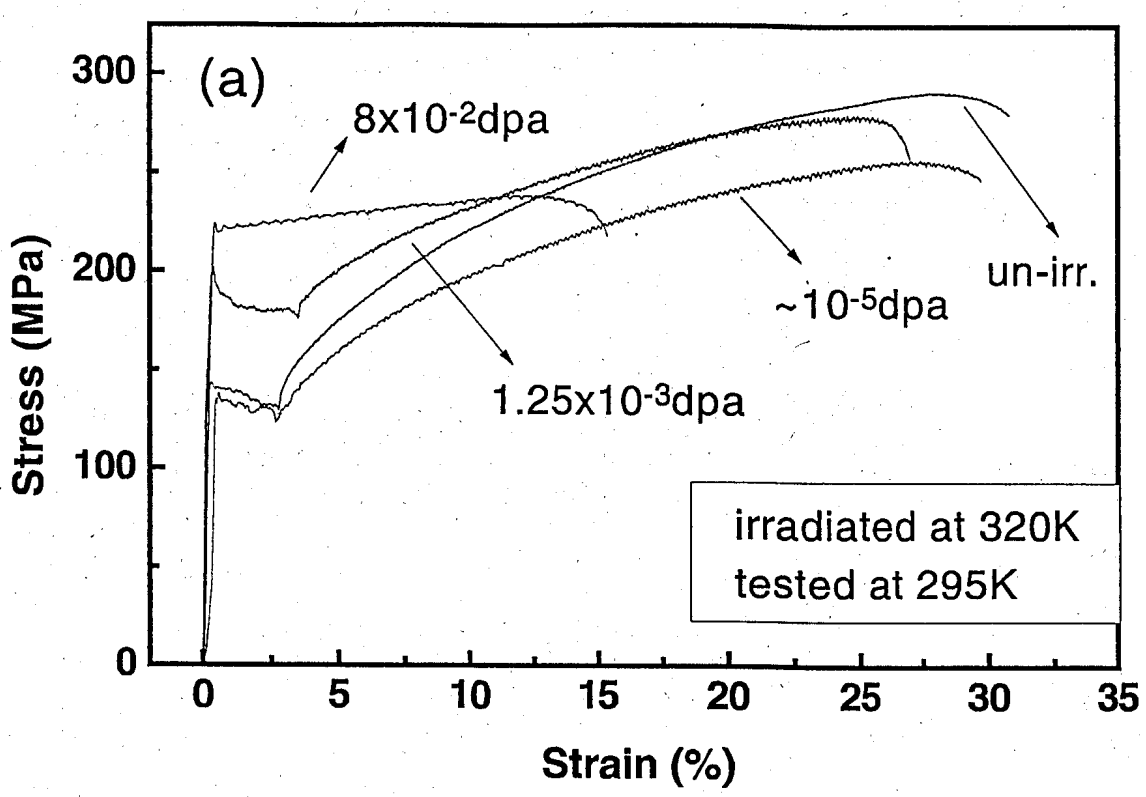
(a)
8x10-2dpa
~10-5dpa
un-irr.
1.25x10-3dpa
irradiated at 320K
tested at 295K
Stress (MPa)
Strain (%)
0
100
200
300
0
5
10
15
20
25
30
35

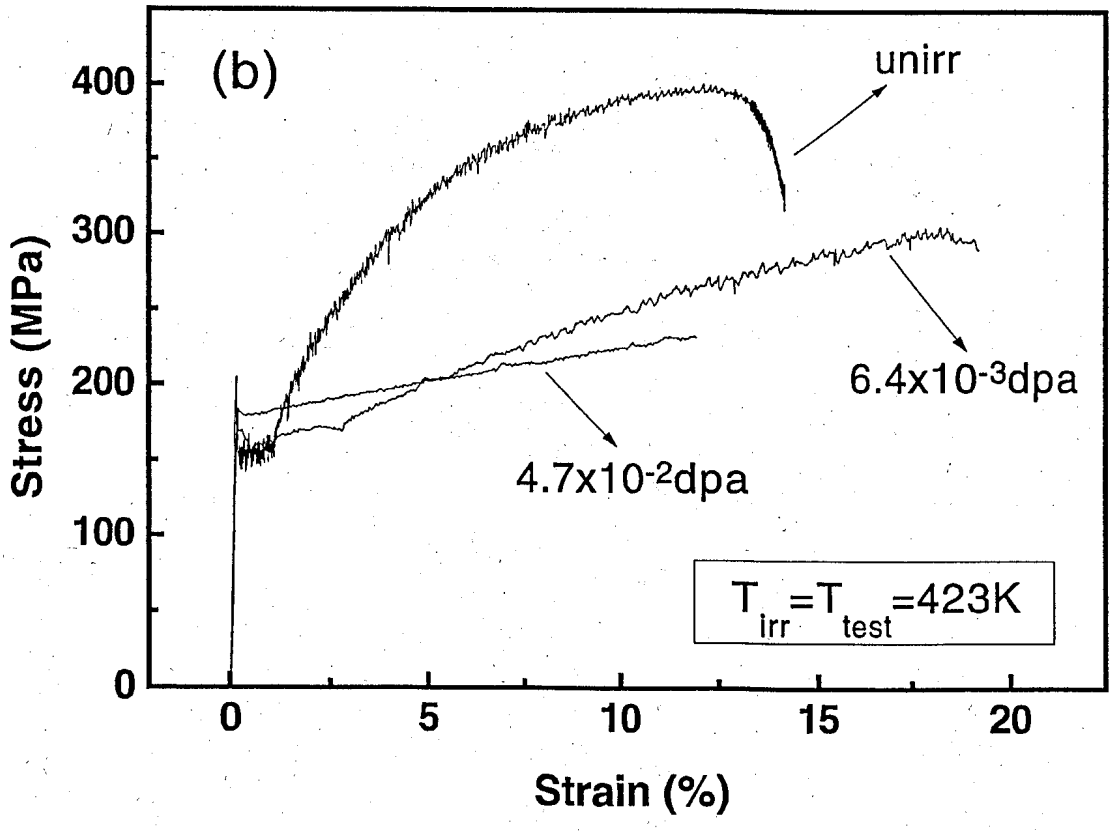
(b)
unirr
6.4x10-3dpa
4.7x10-2dpa
Tirr=Ttest=423K
Stress (MPa)
Strain (%)
0
100
200
300
400
0
5
10
15
20

Fig. 2

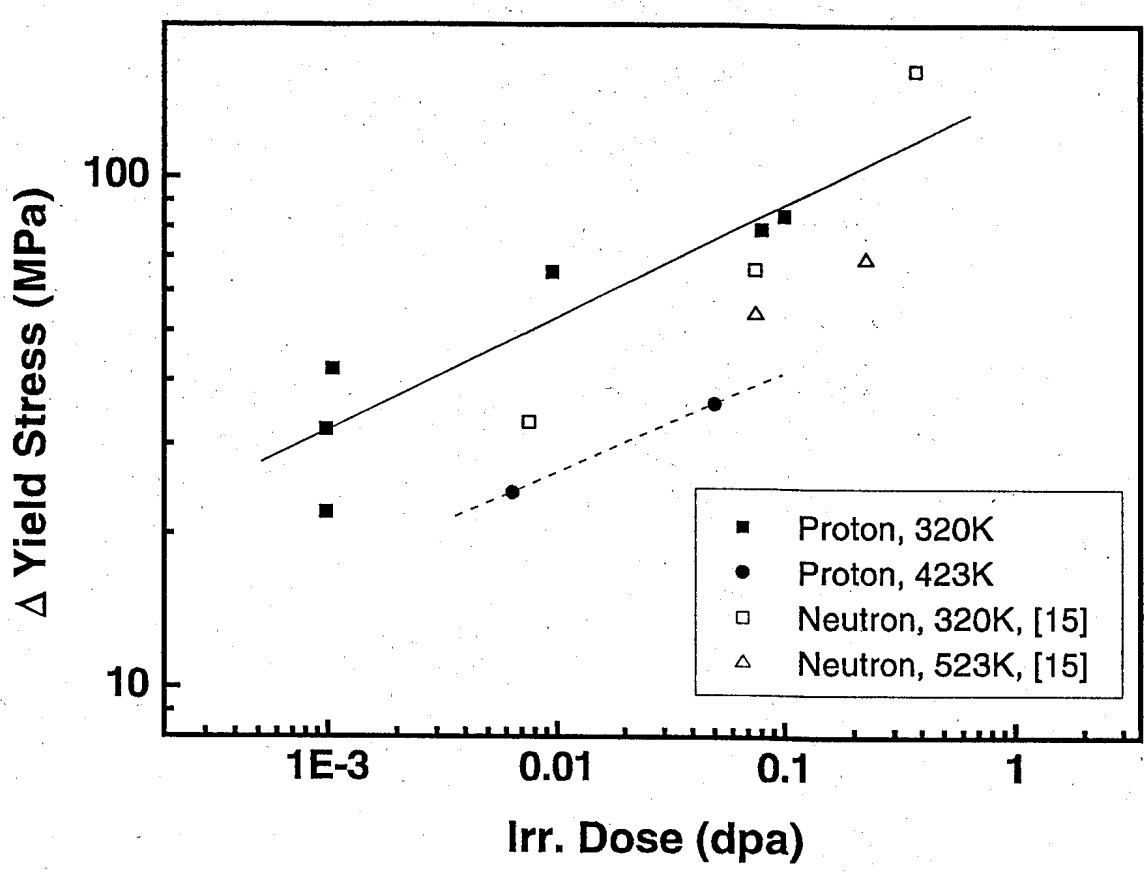
Δ Yield Stress (MPa)
100
10
1E-3
0.01
0.1
1
Irr. Dose (dpa)
Proton, 320K
Proton, 423K
Neutron, 320K, [15]
Neutron, 523K, [15]

Fig. 3

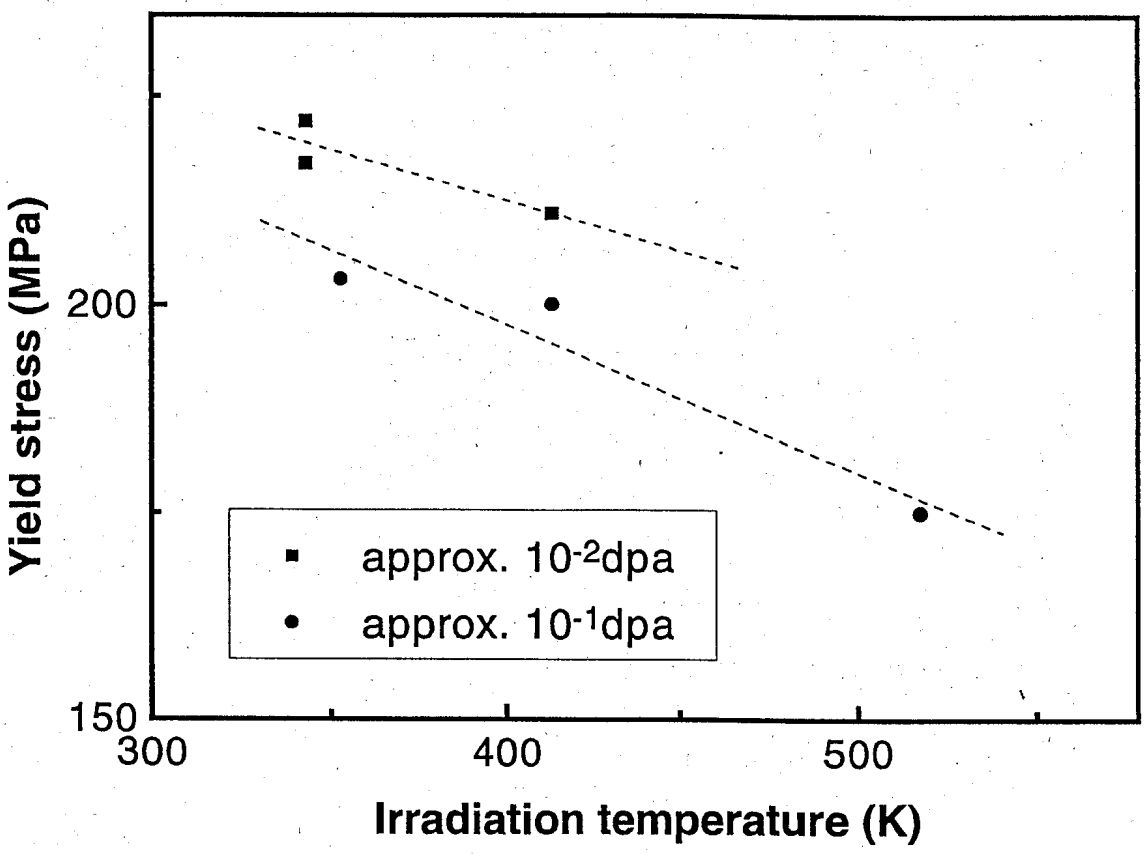
Yield stress (MPa)
200
150
300
400
500
Irradiation temperature (K)
approx. 10-2dpa
approx. 10-1dpa

Fig. 4

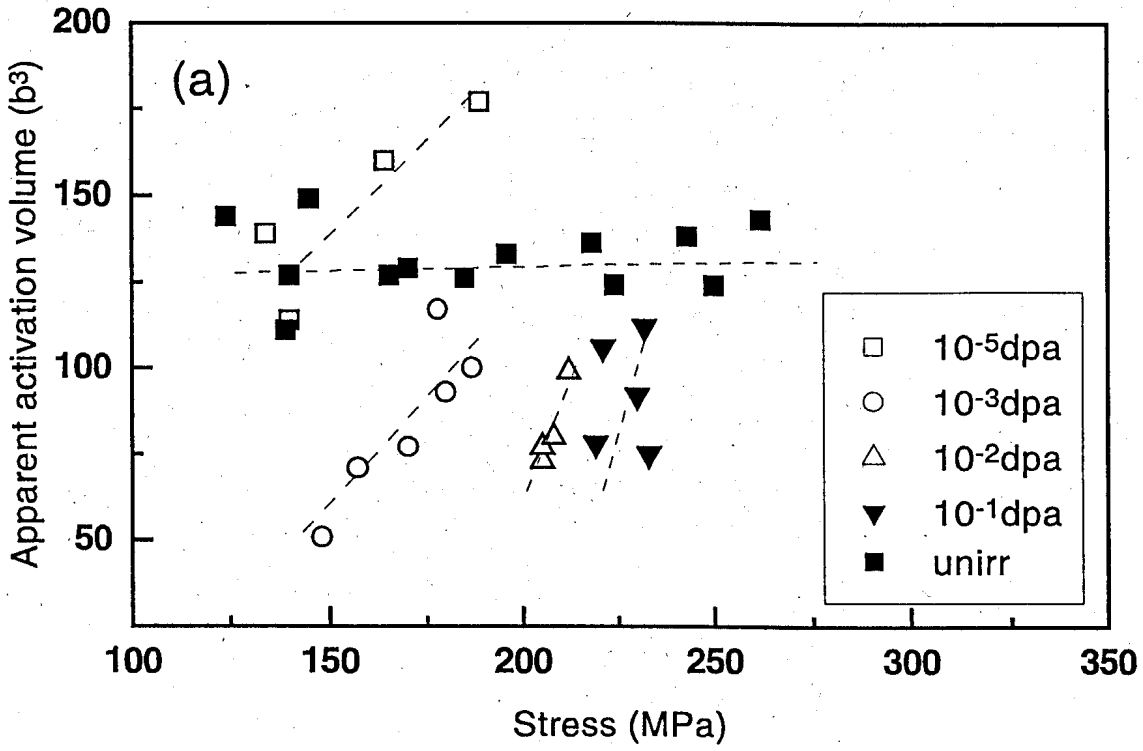
(a)
Apparent activation volume (b³)
200
150
100
50
100
150
200
250
300
350
Stress (MPa)
10⁻⁵dpa
10⁻³dpa
10⁻²dpa
10⁻¹dpa
unirr

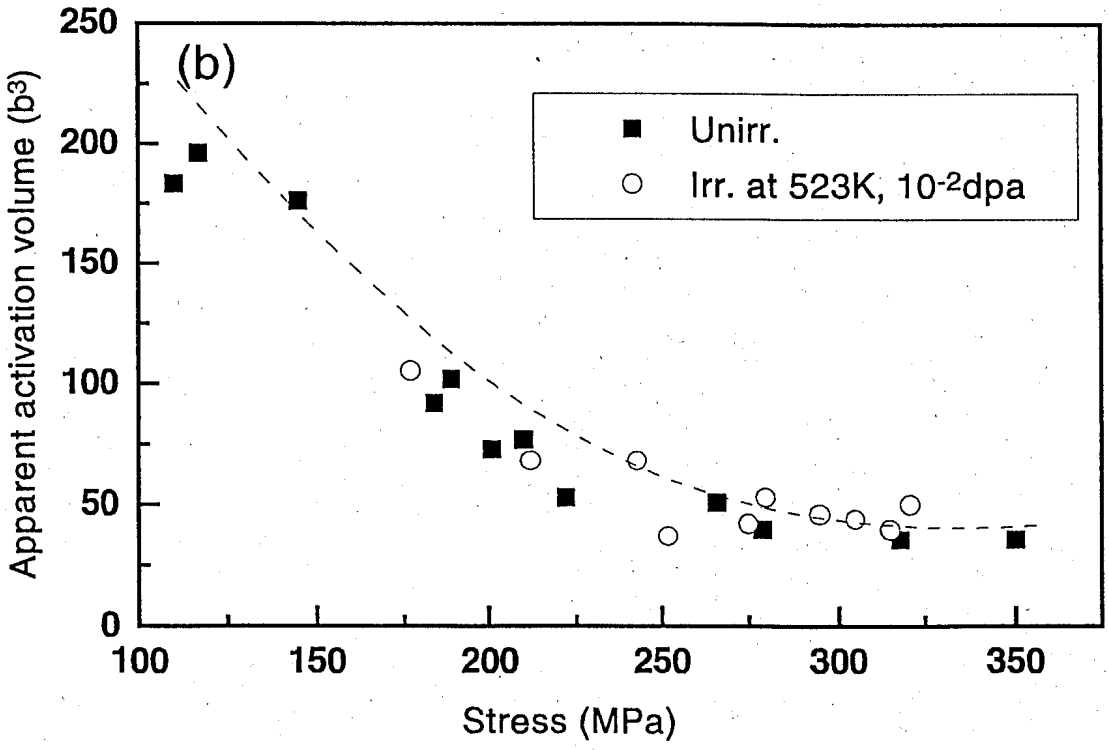
(b)
Apparent activation volume (b³)
250
200
150
100
50
0
100
150
200
250
300
350
Stress (MPa)
Unirr.
Irr. at 523K, 10⁻²dpa

Fig. 5

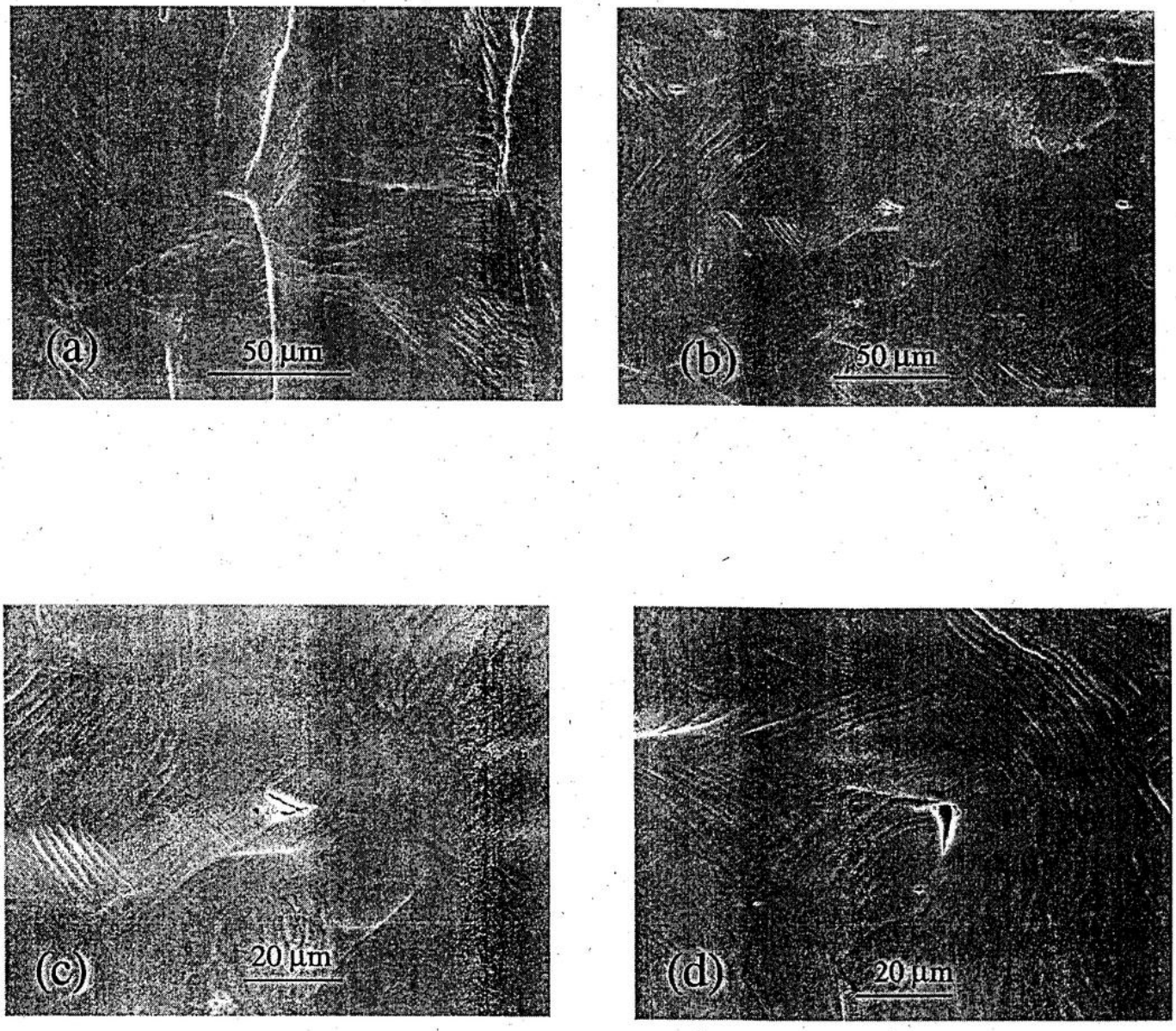

Fig. 6